

Demonstration of a Simple Entangling Optical Gate and Its Use in Bell-State Analysis

N. K. Langford,^{1,2} T. J. Weinhold,^{1,2} R. Prevedel,^{1,2,3} K. J. Resch,² A. Gilchrist,^{1,2}
J. L. O'Brien,^{1,2} G. J. Pryde,^{1,2} and A. G. White^{1,2}

¹Centre for Quantum Computer Technology, University of Queensland, Brisbane QLD 4072, Australia

²Department of Physics, University of Queensland, Brisbane QLD 4072, Australia

³Institut für Experimentalphysik, Universität Wien, Boltzmannngasse 5, 1090 Vienna, Austria

(Received 30 June 2005; published 18 November 2005)

We demonstrate a new architecture for an optical entangling gate that is significantly simpler than previous realizations, using partially polarizing beam splitters so that only a *single* optical mode-matching condition is required. We demonstrate operation of a controlled-Z gate in both continuous-wave and pulsed regimes of operation, fully characterizing it in each case using quantum process tomography. We also demonstrate a fully resolving, nondeterministic optical Bell-state analyzer based on this controlled-Z gate. This new architecture is ideally suited to guided optics implementations of optical gates.

DOI: 10.1103/PhysRevLett.95.210504

PACS numbers: 03.67.Lx, 03.65.Wj, 03.67.Mn, 42.50.Dv

A key resource for using entanglement in quantum information protocols is gates that are capable of entangling or disentangling qubits [1]. Entangling gates lie at the heart of quantum computation protocols, for example, and disentangling gates used in Bell-state analyzers are required for quantum teleportation. Conceptually, the simplest such two-qubit gate is the controlled-Z (CZ) gate, which in the logical basis produces a π phase shift on the $|11\rangle$ term, (i.e., $|00\rangle \rightarrow |00\rangle$; $|01\rangle \rightarrow |01\rangle$; $|10\rangle \rightarrow |10\rangle$; $|11\rangle \rightarrow -|11\rangle$). This is a maximally entangling gate which, when coupled with single-qubit rotations, is universal for quantum computing [2].

In 2001, Knill, Laflamme, and Milburn proposed a scheme for linear optical quantum computing which used measurement to nondeterministically realize the optical nonlinearity required for two-qubit entangling gates [3]. They also showed that deterministic versions of these gates could be achieved using teleportation [4], which requires Bell-state measurement. Since then, there have been a number of demonstrations of quantum logic gates derived from this concept [5–9] and further theoretical development of linear-optics schemes [10–14]. In particular, there is a recent suggestion to use nondeterministic CZ gates to construct cluster states for demonstrating optical cluster-state quantum computation [15].

Here we report an experimental demonstration of a nondeterministic linear-optics CZ gate and its application as a Bell-state analyzer. This CZ gate is the simplest entangling (or disentangling) linear-optics gate realized to date, requiring only three partially polarizing beam splitters (PPBSs), two half-wave plates, no classical interferometers, and no ancilla photons. It is nondeterministic, and success is heralded by detection of a single photon in each of the outputs. We demonstrate the operation of this type of gate using photons generated both by continuous-wave (cw) and by femtosecond-pulsed parametric down-conversion—we find that temporal mode mismatch was not a significant factor in the gate's performance. We fully characterize the operation in both regimes using quantum

process tomography, and we also demonstrate the use of this kind of gate for fully resolving Bell measurements. This simple entangling optical gate is promising for micro-optics or guided optics implementations where extremely good nonclassical interference is realizable.

The best performing entangling gate implementations to date have been interferometric: A conceptual schematic of an interferometric optical CZ gate, composed of three partially reflecting beam splitters with reflectivity $\eta = 1/3$, is shown in Fig. 1(a). Each polarization qubit input to the gate is split into two longitudinal spatial modes via a polarizing beam splitter. The horizontally polarized modes meet at a $1/3$ beam splitter, and nonclassical interference means that, for an arbitrary input state, the entire circuit performs

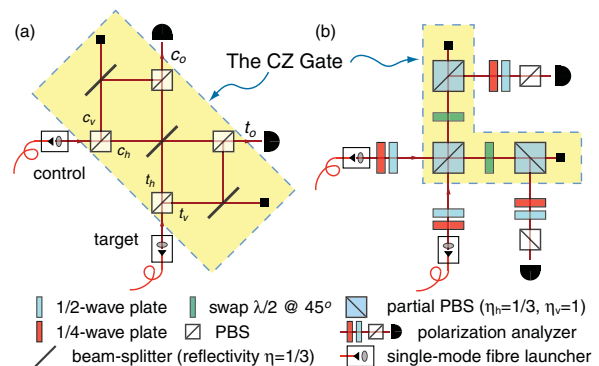


FIG. 1 (color). (a) Interferometric CZ gate based on the approach of Refs. [13,14]. Gate operation is enabled by transforming each qubit from polarization to spatial encoding and back again. This requires high interferometric stability and spatiotemporal mode matching for correct operation. (b) Partially polarizing beam splitter gate. The qubits can remain polarization encoded, since the vertically polarized modes are completely reflected by the first PPBS and do not interact. Nonclassical interference occurs between the horizontally polarized modes, with $\eta = 1/3$. The subsequent PPBSs give the required losses in the c_v and t_v modes as shown in (a).

the transformation: $\alpha|HH\rangle + \beta|HV\rangle + \gamma|VH\rangle + \delta|VV\rangle \rightarrow \frac{1}{3}[-\alpha|HH\rangle + \beta|HV\rangle + \gamma|VH\rangle + \delta|VV\rangle] + \dots$, where H and V refer to horizontal and vertical polarization, respectively, and the terms not shown correspond to the failure mode of the gate (i.e., the control and target output ports do not each contain one photon). With probability $1/9$, the circuit performs the CZ operation (using the logic-basis definitions $0 \equiv V$ and $1 \equiv H$). After the network of $1/3$ beam splitters, the two spatial modes of the control and target must be recombined to return to polarization-encoded qubits. Since the phase relationship between the logical modes must be maintained throughout this operation, interferometric stability is required between the control and target modes. Inherently stable interferometers have previously been used [6,7] to achieve this—however, these may not be suitable for scaling to large numbers in micro- or integrated-optical realizations. Here we take an alternative approach which does not require interferometric stability.

The experimental setup for the CZ gate we have developed is shown schematically in Fig. 1(b). We use PPBSs with reflectivities of $1/3$ and 1 for horizontally and vertically polarized light, respectively [16]. As in Fig. 1(a), only the H modes interfere nonclassically at the first PPBS. The V inputs are then flipped to H by half-wave plates—single-qubit X gates—and are attenuated by the remaining two PPBSs to balance the losses. The circuit of Fig. 1(b) therefore performs a CZ gate with additional X gates on the control and target qubits. These X gates could be corrected with wave plates in the outputs or by relabeling the logical states of the outputs—here we chose to relabel. The key advantage of the PPBS gate is that the polarization modes are never spatially separated and recombined, and, consequently, no classical interference conditions are required. A single nonclassical interference at the first PPBS is, therefore, the gate's sole mode-matching condition.

To test multiqubit circuits, multiphoton sources are required. The current gold standard for generating two or more photons is pulsed parametric down-conversion: Pump power densities far greater than those possible with cw sources lead to significantly higher probabilities of multiphoton events. Down-converted photons from short pump pulses can display more complex interference effects with reduced visibility. Thus, any new gate architecture should be shown to be compatible with both cw and pulsed sources. We tested the PPBS architecture with both cw and

femtosecond-pulsed sources, which produce pairs of energy degenerate single photons via spontaneous parametric down-conversion in a β -barium-borate crystal (Table I). The photon pairs were collected into single mode optical fibers to improve the spatial mode and injected into the CZ gate [Fig. 1(b)]. In the pulsed case, mode-matching was also improved by collecting the gate output into single mode fibers. A pair of half- and quarter-wave plates at the output of each fiber was used for input state preparation. A coincidence window of ~ 5 ns was used, and no correction for accidental counts was made. The gates were completely characterized via quantum process tomography [7,18].

A convenient representation of the measured process is the χ matrix, which is a complete and unique description of the process relative to a given basis of operators. The χ matrix for ideal CZ gate operation in the Pauli basis is shown in Fig. 2(a) (all the components are real). The experimental results for the cw gate are shown in Fig. 2(b), those for the pulsed gate in Fig. 2(c). By using the method of Ref. [7], we are guaranteed physical χ matrices requiring no extra normalization. In the cw case, the Π term is 0.36 instead of the expected 0.25 due to imperfect nonclassical interference resulting from mode mismatch.

Gate performances can be quantified by calculating the process fidelity $F_p = \text{Tr}[\chi_{\text{meas}}\chi_{\text{ideal}}]$ or the average gate fidelity, which is the fidelity between expected and actual output states, averaged over all pure inputs, $\bar{F} = (4F_p + 1)/5$ [7,19]. The cw and pulsed gates have process fidelities of $74.6 \pm 0.3\%$ and $84.0 \pm 0.1\%$, respectively, and average gate fidelities of $79.7 \pm 0.2\%$ and $87.2 \pm 0.1\%$, respectively [20]. Despite more stringent temporal mode-matching requirements in the pulsed regime, the extra spatial filtering led to better gate operation, equivalent to the previous best demonstration [7].

In our experiment, we observed systematic, fixed polarization rotations, probably due to birefringent effects in nonideal PPBSs. In practice, these have no effect on gate quality and, if necessary, could be compensated for with appropriate wave plates. To demonstrate this, we modeled their effect numerically, identifying single-qubit unitary corrections which increased the cw and pulsed process fidelities to $77.0 \pm 0.3\%$ and $86.6 \pm 0.2\%$, respectively, and average gate fidelities to $81.6 \pm 0.2\%$ and $89.3 \pm 0.1\%$, respectively.

A potential drawback of the PPBS architecture is that the beam splitting ratios are fixed at manufacture—in contrast to schemes where the setting of a half-wave plate determines the effective beam splitter reflectivity [6,7]. While the PPBSs for the cw gate (optimized for 702.2 nm) were measured to be within ± 0.01 of the required reflectivities, for the pulsed gate (820 nm), the values for the three PPBSs were $\eta = 0.28, 0.28, \text{ and } 0.29$ (± 0.01 ; normalized to output power). Modeling a gate using 0.28 reflectivities, we find the optimum process fidelity that can be obtained is $F_p^{0.28} = 96\%$ —near ideal. As originally shown in

TABLE I. Photon source parameters.

Parameter	cw	Pulsed
Pump source	Ar ⁺	Doubled Ti:Sa
Pump wavelength	351.1 nm	410 nm
Crystal arrangement	Type I sandwich [17]	Type I single
Photon wavelength	702.2 nm	820 nm
Interference filters	± 0.18 nm	± 1.5 nm
Output state	Separable \leftrightarrow entangled	Separable

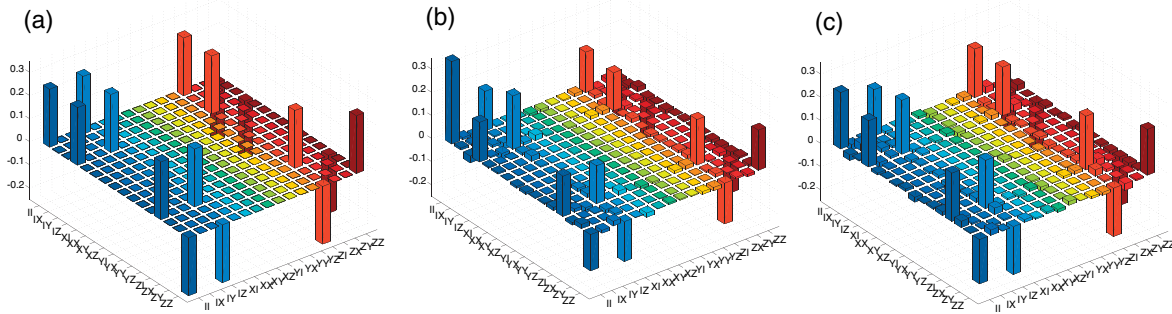


FIG. 2 (color). Quantum process tomography of the CZ gate. Real components of the χ matrix for the: (a) ideal, (b) cw, and (c) pulsed CZ gates. The imaginary components of the experimental matrices are not shown: A few elements are on the order of 0.05; the average is ~ 0.005 .

Ref. [13], the CZ gate is relatively forgiving of the exact splitting ratios, making it an eminently suitable gate to be realized with a PPBS architecture. Performance of the PPBS gates is limited almost exclusively by mode matching, primarily spatial, making these gates promising candidates for micro- or integrated-optical implementations, where nonclassical mode matching in excess of 99% can be expected [21].

We further test the CZ gate by operating it as a Bell-state analyzer of the entangled continuous-wave input states [17]. Because of the geometry of the source, and birefringence and geometric effects in the single mode fibers, the near-maximally entangled state produced is of the form $|HH\rangle + e^{i\varphi}|VV\rangle$. We use quantum state tomography

[22,23] to characterize the source state [Fig. 3(a)]. The tangle $T = 0.93 \pm 0.01$ and linear entropy $S_L = 0.05 \pm 0.01$ show that this state is highly entangled and highly pure; the fidelity with a maximally entangled state is $F = 98.0 \pm 0.4\%$. We determine that $\varphi = -2.094$ radians, and, by using the input wave plates [Fig. 1(b)] to perform appropriate single-qubit unitaries on each qubit, we can transform the state of Fig. 3(a) to any desired maximally entangled state of linear polarization. In Fig. 3(b), we have produced the state $|HH\rangle + |VV\rangle$ with fidelity $F_{\phi^+} = 96.1 \pm 0.2\%$; $T = 0.96 \pm 0.01$ and $S_L = 0.02 \pm 0.01$.

To quantify the performance of the CZ gate as a Bell-state analyzer, we produced the four maximally entangled states: $|\psi^{\pm}\rangle = |HA\rangle \pm |VD\rangle$; $|\phi^{\pm}\rangle = |HD\rangle \pm |VA\rangle$,

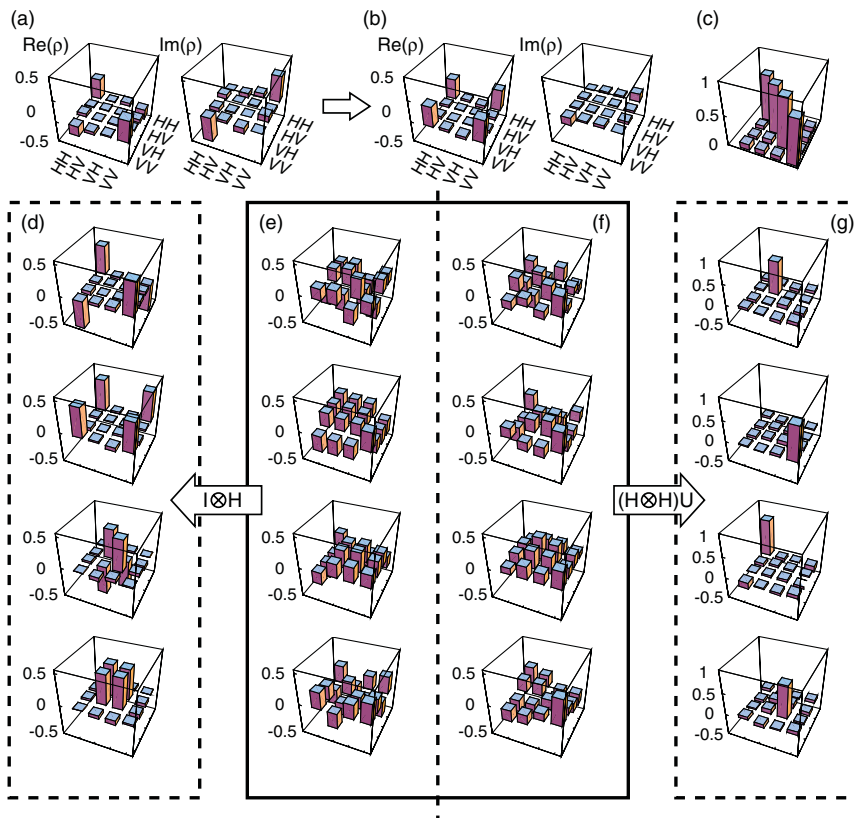


FIG. 3 (color). The CZ gate operating as a Bell-state analyzer. (a) The two-qubit entangled state at the output of the fibers and (b) transformed to the ϕ^+ Bell state. (c) The measured truth table: The average probability of success is 0.78 ± 0.03 . (d)–(g) Transformation of near-maximally entangled states to near-separable states by a CZ gate Bell-state analyzer. (d) The input Bell states determined from (e) the measured input states with the second qubit rotated by a Hadamard. (f) The measured output states, (g) transformed by applying local rotations to each qubit (see text).

where $D \equiv (|H\rangle + |V\rangle)/\sqrt{2}$ and $A \equiv (|H\rangle - |V\rangle)/\sqrt{2}$. These are just the usual four Bell states, with the second qubit rotated by a Hadamard so that they can be discriminated by the CZ gate. The four experimentally produced density matrices are shown in Fig. 3(e): The average of their fidelities is $\bar{F} = 95.8 \pm 0.7\%$; the average of the tangles and linear entropies are $\bar{T} = 0.94 \pm 0.02$ and $\bar{S}_L = 0.04 \pm 0.01$, respectively. For ease of visualization, we have numerically rotated these states into the more familiar form by applying a Hadamard gate to the second qubit [Fig. 3(d)].

An ideal CZ gate would take the four maximally entangled states $|\psi'^{\pm}\rangle, |\phi'^{\pm}\rangle$ to the four separable orthogonal states: $|DD\rangle, |AD\rangle, |DA\rangle$, and $|AA\rangle$, respectively. For the four input states in Fig. 3(e), the measured output density matrices are shown in Fig. 3(f). In fact, they are close to the four orthogonal separable states $(|H\rangle \pm e^{i\varphi_1}|V\rangle) \otimes (|H\rangle \pm e^{i\varphi_2}|V\rangle)$, where $\varphi_1 = -3.07$ and $\varphi_2 = 0.32$ as determined by a best fit. For ease of visualization, we have rotated these states into the logical basis in Fig. 3(g). The average of the fidelities between all combinations of the measured output states is $24 \pm 5\%$ (ideally zero), demonstrating that the states are close to orthogonal. Their average tangle $\bar{T} = 0.04 \pm 0.05$ and linear entropy $\bar{S}_L = 0.42 \pm 0.07$ indicate that they are unentangled, albeit somewhat mixed. This circuit is working quite well as a Bell-state analyzer.

The average fidelity of the measured output states with the above separable states is $F = 79 \pm 3\%$: If we analyzed the output of the circuit in this rotated basis, we would correctly identify the Bell state with a probability of 79%. More directly, we can measure each of the separable states for each Bell-state input by explicitly analyzing in the rotated basis, which gives the directly measured truth table for the CZ gate when operated as a Bell-state analyzer. The results are shown in Fig. 3(c), and the average probability of success is $78 \pm 3\%$, in agreement with the tomography results.

It is interesting to note that, whenever a postselected event occurs, the Bell measurement has effectively discriminated one of four input wave plate settings applied to a single input qubit. That is to say, 2 bits of classical information (representing the four wave plate settings) have been encoded into a single qubit. This is reminiscent of quantum dense coding [24–26], although, because the Bell measurement is nondeterministic, a protocol using this gate would be less efficient than ordinary classical communication. Nevertheless, this still demonstrates the power of entanglement for dense coding given a deterministic Bell analyzer, such as can be constructed, in principle, using measurement-induced nonlinearity.

In summary, we have proposed and demonstrated a new architecture for entangling optical gates. The key advantage of this new gate architecture is its simplicity and suitability for scaling—it requires only one nonclassical mode-matching condition and no classical interferometers. This is very promising for micro-optic and integrated-optic

realizations of this gate, where extremely good mode matching can be expected. Finally, we have demonstrated the operation of this gate as a Bell-state analyzer which has the advantage of higher success probability and no ancilla compared to alternative recent demonstrations [9,27].

This work was supported by the Australian Research Council (ARC), the Queensland Government, and the U.S. Advanced Research and Development Agency (ARDA). R.P. acknowledges support from the Austrian Science Foundation (FWF). We acknowledge Rohan Dalton for valuable discussions.

-
- [1] M. A. Nielsen and I. L. Chuang, *Quantum Computation and Quantum Information* (Cambridge University Press, Cambridge, England, 2000).
 - [2] The more familiar CNOT gate is formed by applying a Hadamard gate H to the target qubit before and after a CZ gate.
 - [3] E. Knill, R. Laflamme, and G. J. Milburn, *Nature (London)* **409**, 46 (2001).
 - [4] D. Gottesman and I. L. Chuang, *Nature (London)* **402**, 390 (1999).
 - [5] T. B. Pittman *et al.*, *Phys. Rev. A* **68**, 032316 (2003).
 - [6] J. L. O'Brien *et al.*, *Nature (London)* **426**, 264 (2003).
 - [7] J. L. O'Brien *et al.*, *Phys. Rev. Lett.* **93**, 080502 (2004).
 - [8] S. Gasparoni *et al.*, *Phys. Rev. Lett.* **93**, 020504 (2004).
 - [9] Z. Zhao *et al.*, *Phys. Rev. Lett.* **94**, 030501 (2005).
 - [10] T. C. Ralph *et al.*, *Phys. Rev. A* **65**, 012314 (2002).
 - [11] E. Knill, *Phys. Rev. A* **66**, 052306 (2002).
 - [12] T. B. Pittman, B. C. Jacobs, and J. D. Franson, *Phys. Rev. Lett.* **88**, 257902 (2002).
 - [13] T. C. Ralph *et al.*, *Phys. Rev. A* **65**, 062324 (2002).
 - [14] H. F. Hofmann and S. Takeuchi, *Phys. Rev. A* **66**, 024308 (2002).
 - [15] M. A. Nielsen, *Phys. Rev. Lett.* **93**, 040503 (2004).
 - [16] The PPBSs are cube beam splitters with appropriately specified multilayered dielectric stacks purchased from Asahi Spectra (702.2 nm) and Special Optics (820 nm).
 - [17] P. G. Kwiat *et al.*, *Phys. Rev. A* **60**, R773 (1999).
 - [18] This involves inputting identical ensembles of 16 separable states into the circuit and performing a set of 36 measurements for each—36 measurements form an overcomplete set which increases accuracy.
 - [19] A. Gilchrist, N. K. Langford, and M. A. Nielsen, *Phys. Rev. A* **71**, 062310 (2005).
 - [20] The errors were estimated by doing a 1000 run Monte Carlo simulation of the whole process tomography analysis, with Poissonian noise added to the count statistics in each run.
 - [21] T. B. Pittman and J. D. Franson, *Phys. Rev. Lett.* **90**, 240401 (2003).
 - [22] A. G. White *et al.*, *Phys. Rev. Lett.* **83**, 3103 (1999).
 - [23] D. F. V. James *et al.*, *Phys. Rev. A* **64**, 052312 (2001).
 - [24] C. H. Bennett and S. J. Wiesner, *Phys. Rev. Lett.* **69**, 2881 (1992).
 - [25] T. Schaez *et al.*, *Phys. Rev. Lett.* **93**, 040505 (2004).
 - [26] K. Mattle *et al.*, *Phys. Rev. Lett.* **76**, 4656 (1996).
 - [27] P. Walther and A. Zeilinger, *Phys. Rev. A* **72**, 010302(R) (2005).